

# The nuclei of radio galaxies in the UV: the signature of different emission processes<sup>1</sup>

Marco Chiaberge<sup>2</sup>, F. Duccio Macchetto<sup>3</sup>, William B. Sparks

*Space Telescope Science Institute, 3700 San Martin Drive, Baltimore, MD 21218*

chiab@stsci.edu

Alessandro Capetti

*Osservatorio Astronomico di Torino, Strada Osservatorio 20, I-10025 Pino Torinese, Italy*

Mark G. Allen

*Space Telescope Science Institute, 3700 San Martin Drive, Baltimore, MD 21218*

and

André R. Martel

*Department of Physics and Astronomy, Johns Hopkins University, 3400 N. Charles Street, Baltimore, MD 21218*

## ABSTRACT

We have studied the nuclei of 28 radio galaxies from the 3CR sample in the UV band. Unresolved nuclei (central compact cores, CCC) are observed in 10 of the 13 FR I, and in 5 of the 15 FR II. All sources that do not have a CCC in the optical, do not have a CCC in the UV. Two FR I (3C 270 and 3C 296) have a CCC in the optical but do not show the UV counterpart. Both of them show large dusty disks observed almost edge-on, possibly implying that they play a role in obscuring the nuclear emission. We have measured optical–UV spectral indices  $\alpha_{\text{o,UV}}$  between  $\sim 0.6$  and  $\sim 7.0$  ( $F_{\nu} \propto \nu^{-\alpha}$ ). BLRG have the flattest spectra and their values of  $\alpha_{\text{o,UV}}$  are also confined to a very narrow range. This is consistent with radiation produced in a geometrically thin, optically thick accretion disk. On the other hand, FR I nuclei, which are most plausibly originated by synchrotron emission from the inner relativistic jet, show a wide range of  $\alpha_{\text{o,UV}}$ . There is a clear trend with orientation in that sources observed almost edge-on or with clear signs of dust absorption have the steepest spectra. These observations imply that in FR I obscuration can be present, but the obscuring material is not in a “standard” geometrically thick torus. The most striking difference between these absorbing structures and the classic AGN “tori” resides in the lower optical depth of the FR I obscuring material.

*Subject headings:* galaxies: active — galaxies: nuclei — ultraviolet: galaxies — radiation mechanism: general

---

<sup>2</sup>ESA fellow

<sup>3</sup>On assignment from ESA

<sup>1</sup>Based on observations obtained at the Space Telescope Science Institute, which is operated by the Association of

---

Universities for Research in Astronomy, Incorporated, under NASA contract NAS 5-26555.

## 1. Introduction

In the framework of the unification models for radio-loud active galactic nuclei, radio galaxies are believed to be the misoriented counterparts of quasars and blazars (Barthel 1989; for a review, see Urry & Padovani 1995). Although observationally this scheme is mainly supported by the comparison of the extended components of these classes of AGN, a direct study of their nuclear properties is a crucial tool both to confirm such a framework, and to infer fundamental information about the innermost structure of these sources.

In quasars and blazars, the nuclear components dominate the observed radiation. Their origin is generally believed to reside in thermal emission from the accretion disk and non-thermal emission from the relativistic jet, respectively. In the case of blazars, the jet is observed almost along its axis and its emission is strongly enhanced by relativistic beaming (Antonucci & Ulvestad 1985). In radio galaxies, all of these components should still be present, although the presence of obscuring structures in the inner few pc, which is strictly required by the unification models at least in the case of the most powerful sources (FR II), might hamper their direct observation. Moreover, the inner jet emission should be strongly de-amplified in radio galaxies, due to the much larger angle of the line-of-sight to jet direction.

The detection of faint nuclear optical components (central compact cores, CCC, or “nuclei”) in 3CR radio galaxies, which are still unresolved even in HST images (Chiaberge et al. 1999, hereafter Paper I) allow us to directly investigate the properties of the optical emission from the active nucleus in this class of sources.

The picture which emerges from these studies is that nearby radio galaxies’ nuclei have two main flavors. A large fraction of FR II appear to be consistent with the currently accepted scheme: they either show strong optical nuclei associated with narrow and broad emission lines, or absorbed nuclei (either not detected or seen through scattered light) in objects with only narrow emission lines (Chiaberge et al. 2002; Chiaberge et al. 2000, hereafter Paper II). On the other hand, most FR I have unobscured synchrotron-dominated optical nuclei, low-efficiency radiating accretion disks (e.g. Advection Domi-

nated Accretion Flows, ADAF, Rees et al. 1982, Narayan & Yi 1995) and lack substantial emission lines regions. Surprisingly, a significant fraction of FR II in which broad lines are not detected, show faint optical nuclei with optical–radio properties undistinguishable from those of FR I. The nature of these sources is still unclear, although their consistency with the FR I nuclei suggests that at least some of them might be unobscured synchrotron nuclei as well. These results have found support in the recent observations by Whysong & Antonucci (2001) of a strong  $10\mu$  nuclear thermal component in Cygnus A (3C 405, an FR II), which is not observed in M 87 (3C 274, an optically unobscured FR I; see also Perlman et al. 2001).

In light of these results, a classification of radio galaxies based on their nuclear properties seems to be more closely related to the physical process occurring in the central regions of the sources rather than in the old FR I/FR II morphological dichotomy. This appears to be (at least qualitatively) consistent with the dual–population scheme proposed recently (Jackson & Wall 1999), which unifies the different sources mainly on the basis of their spectral properties.

However, due to the lack of complete spectral information on the nuclei, several questions are still waiting for a definitive answer: are FR I and FR II nuclei intrinsically different? What is the role of obscuration in FR I? What is the role of the different “flavors” of radio galaxies in the AGN paradigm?

In this paper, we test the nature of radio galaxy nuclei, using HST/STIS UV observations. High resolution UV data are crucial in order to test the new picture of the radio galaxy dichotomy. In view of the relatively low intensity of the underlying stellar emission from the host galaxy the detection of CCC in UV images is straightforward. Due to the reasonably large difference in frequency between UV and optical data, we can derive the spectral shape in this critical region, where different spectral properties are expected for different origins of the observed nuclear components. Furthermore, UV emission is very sensitive to obscuration by dust, therefore the presence of an even moderate amount of absorption along the line of sight to the nuclei will clearly affect their observed spectral properties.

The paper is organized as follows: in Section 2

we describe the sample and the HST observations; in Section 3 we outline our method for the detection and photometry of the nuclei in the UV images, and compare it to what has been done in the optical. In Section 4 we show our results and we combine them with the available radio and optical nuclear data, while in Section 5 we discuss the implications of our results for the nuclear structure and the origin of the emission. In Section 6 we present a summary of our findings and we draw conclusions.

## 2. The sample and the HST observations

We analyze a sample of nearby ( $z < 0.1$ ) FR I and FR II radio galaxies belonging to the 3CR catalog, for which both optical and UV HST observations are available. The sample comprises 28 radio galaxies, 13 of them morphologically classified as FR I and 15 as FR II. Of the 15 FR II, 7 are HEG (high excitation galaxies), 5 are LEG (low excitation galaxies; Hine & Longair 1979, Jackson & Rawlings 1997) and 3 are broad-line radio galaxies (BLRG). The list of the sources is shown in Table 1.

All objects, except for 3C 78, 3C 264 and M 87<sup>4</sup>, have been observed with the HST as part of the STIS UV snapshot survey of 3CR radio sources (Allen et al. 2002). We have excluded from the sample 3C 231 (M 82) which is a starburst galaxy. STIS observations have been made with the NUV-MAMA detector and filters with peak sensitivity at  $\sim 2300$  Å. In particular, most of the images were obtained with the F25SRF2 long pass filter, which excludes strong contamination from the Ly $\alpha$  emission line within the redshift range of our sources. The brightest objects have been observed with the narrower band F25CN182 filter, in order to avoid saturation. M 87, and 3C 78 have also been observed by STIS NUV-MAMA, using the F25QZ filter (whose characteristics are similar to F25SRF2) while 3C 264 has been observed using the F25CN182 filter.

The log of optical and UV observations is presented in Table 2 where it can be seen that for 4 sources (M 87, 3C 78, 3C 264 and 3C 317) the observations occurred simultaneously (or near-

simultaneously). Given that all sources in the sample are likely to be intrinsically variable, the time lapse between observations of the other 24 sources might be significant and we discuss this point further in section 5.3.

The sample is not statistically complete, because a few sources were not observed during the SNAPSHOT campaign. However, all the different spectral and morphological types present in 3CR radio galaxies with  $z < 0.1$  are well represented.

## 3. Detection and photometry of UV CCC

As shown in detail by Allen et al. (2002) the morphology of radio galaxies as observed in the UV band can be significantly different from what is seen in the optical images. This certainly holds in the nuclear region, where dust features dramatically absorb the underlying emission in the UV and clumps of (likely) star formation are present. Also, in that band the stellar emission from the host galaxy is substantially reduced with respect to optical (R-band) frequencies, typically by a factor of  $\sim 15$ , in an  $F_\lambda$  representation.

Most of the UV images have very low level of stellar emission. Therefore, while the search for optical CCC has been based on the analysis of the surface brightness profiles of the central regions of the galaxies (Papers I & II), here we search directly for the UV counterparts of the optical CCC. In addition, we also search for unresolved UV CCC in galaxies which do not have optical CCC, but find none. All of the UV CCC sources have FWHM  $\sim 0.05'' - 0.07''$ , indicating that they are unresolved by HST.

Of the 13 FR I galaxies in our sample, 10 (or 77% of the sample) have a UV nucleus. In the optical, 12 (92%) have a CCC. Whenever a galaxy has a nucleus in the UV, it also has a nucleus in the optical. Of all the FR Is in the sample, only 3C 305 does not have a CCC either in the optical or in the UV. Interestingly, the two sources which lack the UV CCC but do have it in the optical (namely 3C 270 and 3C 296) have prominent nuclear dusty disks observed almost edge on (Capetti & Celotti 1999; Martel et al. 2000). These disks are clearly visible in both the optical and the UV images.

Of the 15 FR II galaxies of our sample, only 5 sources have a nucleus in the UV. All of them

<sup>4</sup>3C 78 and 3C 264 have been observed with STIS as part of program 8233, while M 87 have been observed as part of program 8140, P.I. J. Biretta

TABLE 1  
THE SAMPLE

Name	Morph. Class.	Spectral Class.	redshift $z$	$F_r$ mJy	Opt CCC	UV CCC
3C 29	FR I	–	0.0448	93.0	YES	YES
3C 35	FR II	LEG	0.0670	22.68	NO	NO
3C 40	FR II	LEG	0.0180	626.9	NO	NO
3C 78	FR I	–	0.029	964	YES	YES
3C 66B	FR I	–	0.0215	182.0	YES	YES
3C 192	FR II	HEG	0.0600	8.1	NO	NO
3C 198	FR II	HEG	0.0820	–	YES	YES
3C 227	FR II	BLRG	0.0860	23.23	YES	YES
3C 236	FR II	LEG	0.0990	190	NO	NO
3C 264	FR I	–	0.0206	200.0	YES	YES
3C 270	FR I	–	0.0074	308.0	YES	NO
3C 274 (M 87)	FR I	–	0.0037	4000.0	YES	YES
3C 285	FR II	HEG	0.0790	7.7	YES	NO
3C 293	FR II	LEG	0.0452	100.0	NO	NO
3C 296	FR I	–	0.0237	77.0	YES	NO
3C 305	FR I	–	0.0410	29.5	NO	NO
3C 310	FR I	–	0.0540	80.0	YES	YES
3C 317	FR I	–	0.0342	391.0	YES	YES
3C 321	FR II	HEG	0.0960	37.5	NO	NO
3C 326	FR II	LEG	0.0890	15.7	NO	NO
3C 338	FR I	–	0.0303	105.0	YES	YES
3C 353	FR II	LEG	0.0300	203.5	NO	NO
3C 382	FR II	BLRG	0.0580	217.4	YES	YES
3C 388	FR II	LEG	0.0910	75.67	YES	YES
3C 390.3	FR II	BLRG	0.0560	414	YES	YES
3C 449	FR I	–	0.0181	37.0	YES	YES
3C 452	FR II	HEG	0.0810	150	NO	NO
3C 465	FR I	–	0.0301	270.0	YES	YES

Classifications and data from the literature for the sample of 3CR radiogalaxies. (1) 3C name of the source; (2) radio morphological classification; (3) optical spectral classification, as taken from Jackson & Rawlings (1997); (4) Redshift (from NED); (5) radio core flux at 5 GHz collected from the literature (Giovannini et al. 1988, Zirbel & Baum 1995); (6) and (7) presence/absence of a CCC in the HST images (from Paper I, Paper II, Allen et al. 2001 and this work).

TABLE 2  
LOG OF HST OPTICAL AND UV OBSERVATIONS

Name	Instrument	Filter	Obs. date	Instrument	Filter	Obs. Date
3C 29	WFPC2	F702W	Jan 12 1995	STIS NUV-MAMA	F25SRF2	Jun 08 2000
3C 35	WFPC2	F702W	Mar 12 1994	STIS NUV-MAMA	F25SRF2	Oct 10 1999
3C 40	WFPC2	F702W	Jul 18 1994	STIS NUV-MAMA	F25SRF2	Jun 06 2000
3C 66B	WFPC2	F814W	Jan 31 1999	STIS NUV-MAMA	F25SRF2	Jul 13 2000
3C 78	STIS CCD	F28X50LP	Mar 15 2000	STIS NUV-MAMA	F25QTZ	Mar 15 2000
3C 192	WFPC2	F555W	Jan 13 1997	STIS NUV-MAMA	F25SRF2	Mar 23 2000
3C 198	WFPC2	F702W	Mar 20 1994	STIS NUV-MAMA	F25SRF2	Apr 23 2000
3C 227	WFPC2	F702W	May 19 1995	STIS NUV-MAMA	F25SRF2	Jan 25 2000
3C 236	WFPC2	F702W	Oct 19 1994	STIS NUV-MAMA	F25SRF2	Oct 05 1999
3C 264	STIS CCD	F28X50LP	Feb 13 2000	STIS NUV-MAMA	F25CN182	Feb 12 2000
3C 270	WFPC2	F791W	Dec 13 1994	STIS NUV-MAMA	F25SRF2	Mar 05 2000
3C 274	WFPC2	F814W	May 11 1999	STIS NUV-MAMA	F25QTZ	May 17 1999
3C 285	WFPC2	F702W	Feb 05 1994	STIS NUV-MAMA	F25SRF2	Apr 16 2000
3C 293	WFPC2	F702W	Jan 15 1995	STIS NUV-MAMA	F25SRF2	Jun 14 2000
3C 296	WFPC2	F702W	Dec 14 1994	STIS NUV-MAMA	F25SRF2	Apr 15 2000
3C 305	WFPC2	F702W	Sep 04 1994	STIS NUV-MAMA	F25SRF2	Apr 27 2000
3C 310	WFPC2	F702W	Sep 12 1994	STIS NUV-MAMA	F25SRF2	Jun 10 2000
3C 317	FOC	F555W	Mar 05 1994	FOC	F210M	Mar 05 1994
3C 321	WFPC2	F702W	Apr 29 1995	STIS NUV-MAMA	F25SRF2	Jun 05 2000
3C 326	WFPC2	F702W	Apr 29 1995	STIS NUV-MAMA	F25SRF2	Mar 12 2000
3C 338	WFPC2	F702W	Sep 09 1994	STIS NUV-MAMA	F25SRF2	Jun 04 2000
3C 353	WFPC2	F702W	Mar 18 1995	STIS NUV-MAMA	F25SRF2	Jun 22 2000
3C 382	WFPC2	F702W	Jun 25 1994	STIS NUV-MAMA	F25CN182	Feb 23 2000
3C 388	WFPC2	F702W	Sep 18 1994	STIS NUV-MAMA	F25SRF2	Jun 02 2000
3C 390.	WFPC2	F702W	Sep 20 1994	STIS NUV-MAMA	F25CN182	Aug 10 1999
3C 449	WFPC2	F702W	Aug 06 1994	STIS NUV-MAMA	F25SRF2	Apr 16 2000
3C 452	WFPC2	F702W	May 05 1994	STIS NUV-MAMA	F25SRF2	Jan 30 2000
3C 465	WFPC2	F814W	Jul 03 2000	STIS NUV-MAMA	F25SRF2	May 25 2000

also have a CCC in the optical. In particular, a CCC is present in all of the 3 BLRG, and only in 1/5 and 1/7 of the HEG and LEG, respectively. The BLRG have the brightest nuclei of the sample. HST data are available for 3C 285 both in the R and V bands. A faint CCC is present in the R band image, but this component is not detected in the V band. In this case, obscuration might be provided by a prominent large scale dust lane, similar to that observed in Centaurus A. In this latter object, the IR-bright nucleus vanishes in HST images for wavelengths shorter than  $\sim 5000$  Å (Marconi et al. 2000).

We have performed aperture photometry of all the nuclei using the IRAF RADPROF task, setting the background level at a distance of  $\sim 0.17$  arcsec (7 pixels in the STIS/MAMA images) from the center. Counts were converted to fluxes adopting the HST internal calibration<sup>5</sup>, which is accurate to 5%. However, except for those sources in which the CCC is clearly the only observed component in the UV, the dominant source of error is the presence of some extended emission from the host galaxy and/or absorption features which might strongly affect the background determination. This results in a typical error of  $\sim 10\%$ , therefore comparable to that in the optical.

For 3C 270 we derive a rough upper limit to the nuclear flux, as the presence of a dusty disk and emission features in both the optical and UV images allows us to identify the position of the nucleus, although it is not visible in the UV. For the remaining objects no reliable upper limits can be derived. Also note that the LEG 3C 35 has a UV central component which is not a point source.

#### 4. Results

The results of the photometry of the CCC are summarized in Table 3. For completeness, we also

<sup>5</sup>The PHOTFLAM parameter in the image header (inverse sensitivity) is defined assuming a flat spectral distribution in  $F_\lambda$  (in units of  $\text{erg cm}^{-2} \text{s}^{-1} \text{\AA}^{-1}$ ). As we will show in the following, most of the nuclei have significantly sloped spectral indices. We have therefore recalculated the effective observing wavelength and the value of the inverse sensitivity with an iterative process for all of the sources, using the SYNPHOT package. Only in the case of 3C 449, the source with the steepest observed spectrum, this significantly affects the effective observing wavelength and the estimate of the flux.

include the optical fluxes, as taken from Paper I and II. Since in the UV band dust absorption plays an important role in drastically reducing the observed flux, we have de-reddened the fluxes taking into account the galactic absorption and adopting the Cardelli et al. (1988) extinction law (Table 4). In the following sections and figures we will use the de-reddened fluxes, although galactic extinction does not significantly affect the results in any of the sources<sup>6</sup>.

To study the relationship between the optical and UV CCC for the 15 sources of Table 4, we plot their UV flux and luminosity versus their optical values. The same behavior is observed in both the flux and luminosity regimes: we see that the UV CCC span a range of  $\sim 5$  dex in flux and  $\sim 6$  dex in luminosity, whereas the optical CCC span smaller ranges (about 1 dex in both flux and luminosity).

Given the large difference in frequency between the optical (R-band) and UV observations, we could derive the broadband spectral indices [optical–UV] with considerable greater accuracy than previously possible (Paper I). The values of  $\alpha_{o,UV}$ , where  $\alpha$  is defined as  $F_\nu \propto \nu^{-\alpha}$ , are reported in Table 4. Typical errors for  $\alpha$  are of the order of  $\pm 0.1$ . For reference, in Fig 1 and 2 we have overplotted dashed lines corresponding to different optical-UV spectral indices  $\alpha_{o,UV}=1,2,4,6$  (top to bottom). We find that the UV and optical luminosities of the brightest sources are almost identical. However, the lower optical luminosity sources have much weaker UV emission (by a factor of  $\sim 100$ ).

In Fig. 3 we plot the optical-UV spectral index vs. the ratio between the optical CCC and the radio core flux. The quasi-linearity of the FR I radio-optical correlation implies a quasi-constant ratio of the optical to radio flux (corresponding to  $\log(F_o/F_r) \sim -3.6$ ), therefore objects on the left side of this plot are on the FR I correlation, while for higher values of  $\log(F_o/F_r)$  an optical excess is present. The shaded area corresponds to the rms of the correlation (see figure caption for details). Unfortunately, no radio core measurements are available in the literature for 3C 198,

<sup>6</sup>The maximum value of the color excess due to galactic absorption is  $E(B-V) = 0.167$  in the case of 3C 449. This value of  $E(B-V)$  affects the UV and optical fluxes by factors of only 3 and 1.4, respectively.

TABLE 3  
OBSERVED FLUXES OF OPTICAL AND UV CCC

Source name	$F_{opt}$ erg cm <sup>-2</sup> s <sup>-1</sup> Å <sup>-1</sup>	$\lambda_{opt}$ Å	$F_{UV}$ erg cm <sup>-2</sup> s <sup>-1</sup> Å <sup>-1</sup>	$\lambda_{UV}$ Å
FR I				
3C 29	$5.8 \times 10^{-18}$	7000	$2.1 \times 10^{-19}$	2528
3C 66B	$2.7 \times 10^{-17}$	8086	$4.5 \times 10^{-17}$	2528
3C 78	$3.8 \times 10^{-16}$	7216	$2.8 \times 10^{-16}$	2475
3C 264	$1.6 \times 10^{-16}$	7216	$3.0 \times 10^{-16}$	2078
3C 270 <sup>a</sup>	$5.1 \times 10^{-18}$	7930	$< 1.0 \times 10^{-18}$	2528
3C 274	$3.4 \times 10^{-16}$	8086	$3.8 \times 10^{-16}$	2475
3C 310	$3.5 \times 10^{-18}$	7000	$1.6 \times 10^{-18}$	2528
3C 317	$2.0 \times 10^{-17}$	5508	$4.7 \times 10^{-18}$	2213
3C 338	$1.0 \times 10^{-17}$	7000	$3.9 \times 10^{-18}$	2528
3C 449	$1.8 \times 10^{-17}$	7000	$1.9 \times 10^{-19}$	3256
3C 465	$1.0 \times 10^{-17}$	8086	$2.1 \times 10^{-18}$	2528
FR II				
3C 198	$4.9 \times 10^{-17}$	7000	$1.1 \times 10^{-16}$	2528
3C 227	$2.9 \times 10^{-16}$	7000	$5.9 \times 10^{-16}$	2528
3C 382	$4.9 \times 10^{-15}$	7000	$1.6 \times 10^{-14}$	2078
3C 388	$6.7 \times 10^{-18}$	7000	$2.0 \times 10^{-18}$	2528
3C 390.3	$1.1 \times 10^{-15}$	7000	$2.0 \times 10^{-15}$	2078

<sup>a</sup> For 3C 270 an upper limit to the UV CCC has been derived (see section 3).

TABLE 4  
DEREDDENED UV AND OPTICAL DATA OF THE CCC

Source name	Spectr. Class.	$\log F_{opt}$	$\log F_{UV}$	$\log L_{opt}$	$\log L_{UV}$	$\alpha_{o,UV}$	$\sigma_{\alpha}$	E(B-V)
FR I								
3C 29		-27.99	-30.25	26.57	24.31	5.1	0.2	0.036
3C 66B		-27.18	-27.80	26.76	26.13	1.2	0.1	0.080
3C 78		-26.03	-26.74	28.15	27.44	1.5	0.1	0.173
3C 264		-26.54	-27.28	27.36	26.61	1.4	0.1	0.023
3C 270		-27.96	-29.62	25.05	23.39	> 3.4	–	0.018
3C 274		-26.12	-27.05	26.30	25.37	1.8	0.1	0.022
3C 310		-28.21	-29.35	26.50	25.36	2.6	0.1	0.042
3C 317		-27.65	-28.97	26.68	25.35	3.3	0.2	0.037
3C 338		-27.78	-29.05	26.44	25.17	2.9	0.1	0.012
3C 449		-27.38	-29.83	26.40	23.95	7.3	0.2	0.167
3C 465		-27.61	-29.16	26.60	25.06	3.1	0.1	0.069
FR II								
3C 198	HEG	-27.08	-27.56	27.98	27.50	1.1	0.1	0.026
3C 227	BLRG	-26.30	-26.83	28.79	28.26	1.2	0.1	0.026
3C 382	BLRG	-25.03	-25.37	29.74	29.40	0.6	0.1	0.070
3C 388	LEG	-27.89	-29.15	27.25	25.99	2.8	0.2	0.080
3C 390.3	BLRG	-25.68	-26.27	29.06	28.47	1.1	0.1	0.071

Fluxes (in units of  $\text{erg cm}^{-2} \text{s}^{-1} \text{Hz}^{-1}$ ) and luminosities ( $\text{erg s}^{-1} \text{Hz}^{-1}$ ) dereddened taking into account galactic absorption (column (8), from NED).

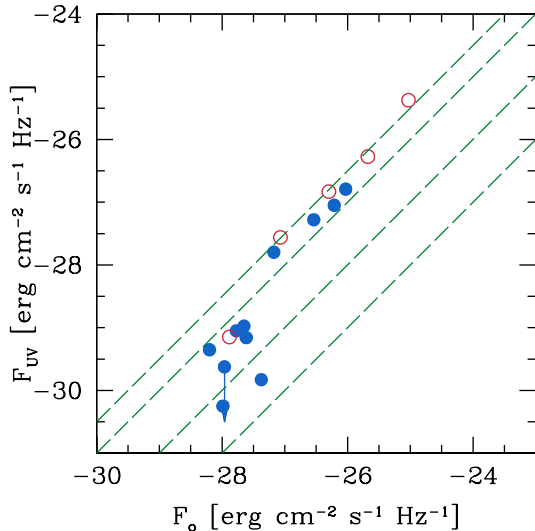


Fig. 1.— UV flux vs. optical flux of the central compact cores. Filled circles are FR I, while FR II are represented as empty circles. The dashed lines represent values of  $\alpha_{o,UV}=1,2,4,6$  (top to bottom).

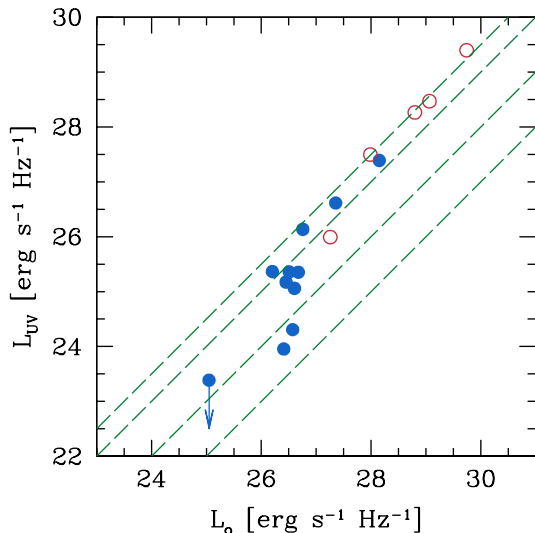


Fig. 2.— UV vs. optical luminosity of the central compact cores. Filled circles are FR I, while FR II are represented as empty circles. The dashed lines represent values of  $\alpha_{o,UV}=1,2,4,6$  (top to bottom).

therefore its position in this plane is undetermined. Sources clearly separate in this plane. Broad-lined FR II have similar (and rather flat)  $\alpha_{o,UV}$ . The synchrotron-dominated FR I have lower values of  $F_o/F_r$  by a factor of ( $\sim 10 - 100$ ), they lie in the region of the correlation between the radio and optical cores, but span a large range in  $\alpha_{o,UV}$ . Interestingly, the only LEG FR II with a detected CCC (3C 388) lies in the region typical of FR I. For comparison, we have also plotted radio-loud QSO<sup>7</sup> with  $z < 0.3$  from the sample of Elvis et al. (1994). Since these sources are at a higher redshift than our 3C galaxies, we have used the I-band magnitudes and the UV fluxes measured at 3000 Å (as taken from Elvis et al. 1994) to mimic the rest-frame  $\alpha_{o,UV}$ . BLRG in our sample and the QSO occupy the same region of the plane, except for 3C 273. In the following we will discuss the implications of the different position of the sources in this plane, strongly supporting a different origin of the nuclear emission in the various classes of radio galaxies.

## 5. Discussion

UV data are a fundamental tool to study the effects of obscuration in the central regions of these galaxies, as this spectral band is very sensitive to the presence of dusty structures. Also, different emission processes for the nuclei imply different values of the optical–UV spectral slopes. By combining the UV data with the already available radio and optical data, we can address some important questions such as:

- are FR I and FR II intrinsically different?
- what do the UV observations tell us about their physical nature?
- what is the role of these sources in the AGN paradigm?
- what is the role of obscuration in FR I?

Qualitatively, FR II nuclei are brighter and have flatter spectral slopes than FR I. Such a behavior can be accounted for by two basic scenarios: (i) an intrinsic spectral difference, reflecting different physical properties, and (ii) an external

<sup>7</sup>The radio-loud QSO with  $z < 0.3$  from the Elvis et al. (1994) sample are: 3C 206 ( $z = 0.197$ ), 3C 323.1 ( $z = 0.264$ ), MC2 1635+119 ( $z = 0.146$ ), PHL 1657 ( $z = 0.2$ ) PG 0007+106 ( $z = 0.089$ ), B2 1028+313 ( $z = 0.178$ ), 3c 273 ( $z = 0.158$ ) and 4C 34.47 ( $z = 0.206$ ).

reason, namely a different amount of absorption in the various sources. Obviously, it is also possible that a combination of these two factors contributes to define the observed properties. Whatever the nature of the CCC, an increasing column density naturally both steepens the spectral slope and lowers the amount of observed photons. However, the physical processes responsible for the emission cannot be constrained on the basis of only the optical and UV fluxes and luminosities.

In the following sections we will further discuss the nature of the CCC by taking advantage of the already known behavior of the different sources in the radio-optical plane.

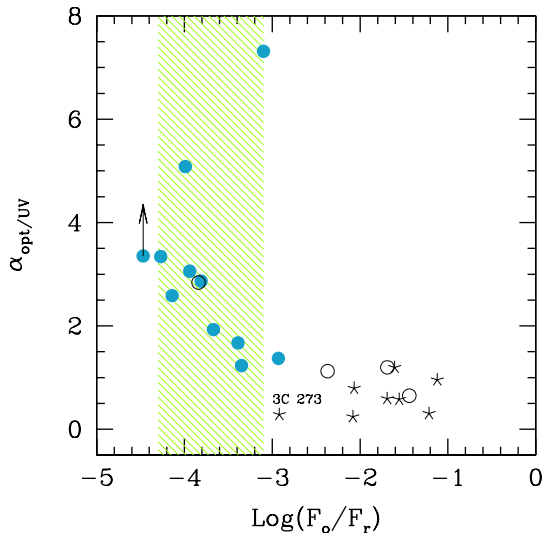


Fig. 3.—  $\alpha_{o,UV}$  versus the logarithm of the ratio between optical CCC flux to radio core flux. Filled circles are FR I, while FR II are represented as empty circles. Stars represent radio-loud quasars from the Elvis et al. 1994 sample. The shaded region corresponds to the  $1\sigma$  dispersion of the radio-optical correlation found for FR I nuclei.

### 5.1. Disk dominated vs. synchrotron dominated sources?

It is widely believed that in radio-loud AGN two main emitting components play a role in defining the optical-UV spectral properties of the nuclear continuum: the thermal emission from the accretion disk and the non-thermal synchrotron

radiation from the relativistic jet. In addition, we must consider the role of absorption, which might significantly alter the observed spectra. Theoretical models for thermal disk emission (in the case of a standard Shakura–Sunyaev, optically thick and geometrically thin disk) predict that such a component should peak in the UV band, at wavelengths shorter than  $1000 \text{ \AA}$ , therefore hard UV spectral slopes ( $\alpha_{UV} \sim 0.3$ ) are expected. Flat spectral components with  $\alpha_{o,UV} < 1$  are indeed commonly observed in both radio-quiet and radio loud QSO (see e.g. Elvis et al. 1994).

On the other hand, the spectral slope of synchrotron dominated sources is poorly constrained, as it depends on physical parameters (mainly on the electron distribution, the magnetic field and the beaming factor) which cannot be easily determined “a priori”. However, we can try to estimate it by analogy with other synchrotron emitting sources for which the SED is well known. In the framework of the AGN unification schemes, radio galaxies are believed to constitute the so-called parent population of blazars, therefore the comparison with the observed properties of these sources might be helpful. Blazars are objects in which the jet is believed to be observed almost “on-axis”. Their observed SED (in a  $\log \nu - \log(\nu F_\nu)$  representation) is composed of two broad peaks: the lower energy peak is commonly interpreted as due to synchrotron emission, while the high energy peak is ascribed to inverse Compton emission. The frequency of the peaks can vary substantially from one source to another: the lower energy peak can be located between the IR and the X-ray band, while the higher energy peak is generally in the gamma-ray band. Fossati et al. (1998) have shown that the position of the synchrotron peak, which is well constrained by the observations, is related to the bolometric luminosity of the source. The lower the power of the object, the higher the synchrotron peak frequency  $\nu_{\text{peak}}$ .

Clearly, the relative position of the peak and the observing frequencies strongly affects the observed UV–optical spectral index. For objects in which  $\nu_{\text{peak}}$  is significantly lower than the observing range, steep ( $\alpha \sim 1 - 3$ ) spectral indices are measured, while flatter spectra ( $\alpha \sim 0.5 - 1$ ) are observed if  $\nu_{\text{peak}}$  is placed at higher frequencies.

Relativistic effects must also be taken into con-

sideration in order to estimate the putative position of the synchrotron peak for our nuclei. Since the emission from the jet is strongly affected by beaming, the peak frequency shifts towards lower values and (most importantly) towards lower luminosities as the angle between the jet axis and the line of sight increases. However, as a result of beaming, it is possible that in highly misoriented objects such as most radio galaxies, the radiation emitted by a slower component of the jet (e.g. a layer) might dominate the observed nuclear emission, while the (faster) component which dominates blazar emission might not be observed (Chiaberge et al. 2000b). Unfortunately, the spectral properties of this component are still very poorly known.

The position of the objects in the plane formed by the optical–UV spectral index vs the logarithm of the ratio between optical CCC flux to radio core flux, which is shown in Fig. 3 and has been described in Sect. 4, can be interpreted as related to the different nature of their nuclear emission. Objects in our sample which show an optical excess with respect to the radio-optical correlation are BLRG FR II and have flatter spectral indices ( $\alpha_{o,UV} \sim 0.6 - 1.2$ ). These sources occupy the same region of the plane as radio-loud quasars of comparable redshift, from the (Elvis et al. 1994) sample, which are plotted as stars. The SED of the QSOs is well known and it clearly shows the presence of a “blue bump”, which is commonly interpreted as the most prominent signature of thermal emission from the accretion disk. The only quasar with a lower value of  $\log(F_o/F_r)$  is 3C 273, which is classified as a blazar. The contribution from the relativistic jet emission (which generally shows strong variations) in this spectral region can indeed alter substantially the observed spectrum in this source (Ghisellini et al. 1998). In fact, it lies close to the region of the FR I correlation, indicating that thermal disk emission is low in the optical band, but shows a flat  $\alpha_{o,UV} < 1$ , implying the presence of a strong component at higher energies, similarly to what is observed in the other QSO.

We conclude that our BLRG are compatible with being thermal-disk dominated objects. Their distance from the shaded region is possibly determined by the relative contribution of the disk and jet emission, which might also be related to the

source orientation.

As pointed out above, FR I show a different behavior. They have similar values of  $F_o/F_r$ , since they lie on the radio-optical correlation, while they span a large range in  $\alpha_{o,UV}$ , from  $\sim 1$  to the extreme case of 3C 449, for which  $\alpha_{o,UV} = 7$ . However, taking into account the above considerations, we can conclude that slopes significantly flatter or steeper than unity are not expected for our sources. Steep spectral slopes in synchrotron spectral components can be observed only for a relatively small range of frequencies, which is confined to be well above the low energy peak, but still before the rising of the inverse-Compton component. Therefore, intrinsic values of  $\alpha_{o,UV}$  larger than  $\sim 3$  appear to be implausible for synchrotron emitting sources. In the following section we show that a moderate amount of absorption can account for the observed behavior.

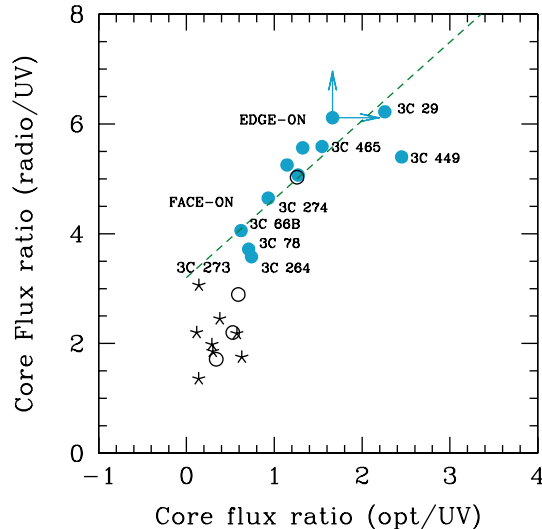


Fig. 4.— The ratio of the radio core to UV CCC flux vs. the ratio of the optical CCC to UV CCC flux. Filled circles are FR I, while FR II are represented as empty circles. Stars represent radio-loud quasars from the Elvis et al. 1994 sample. The dashed line is the absorption trail: less absorbed sources (seen face-on) are on the bottom-left of the plot (section 5.2).

## 5.2. Evidence for a moderate amount of obscuration in FR I

The apparent inconsistency between the synchrotron scenario and the presence of such steep spectral slopes, can be solved if a modest amount of absorption is present, since it might naturally contribute to steepen the observed spectrum. In order to test whether the range of spectral indices and their relative amounts of radio, optical, and UV emission is compatible with being due to absorption, we have plotted in Fig. 4 the ratio of radio to UV emission, versus the ratio between optical and UV emission. The dashed line is the “absorption trail”, which has been calculated by taking into account the effects of an increasing amount of absorption on the observed optical and UV fluxes.

All FR I (except for 3C 449) are well aligned to such a line. The FR II 3C 388 lies on the absorption trail as well. If we assume an intrinsic slope of 1 for all of these sources, the range of observed  $\alpha_{o,UV}$  corresponds to a very small amount of absorption. A maximum  $A_V$  of  $\sim 6$  is obtained in the extreme case of 3C 449, while all other sources are between 0.15 and 3 (the median being  $A_V = 1.3$ ). Although this is a *clear evidence of nuclear absorption in FR I sources*, these observations show that the properties of the absorbing material are not compatible with a standard geometrically thick torus structure. In fact, the position of the sources along the absorption trail in Fig.4 is strictly connected with orientation. On the one hand, the sources which appear to be the less absorbed (namely 3C 264, 3C 66B, 3C 78 and 3C 274, lying on the bottom-left of the plane, close to the BLRG), are all objects in which optical jets are seen. The presence of such features has been interpreted as due to their relatively small viewing angle (Sparks et al. 2000) which, as a result of relativistic beaming, contributes to enhance the jet radiation. On the other hand, dusty disks observed almost edge-on are seen among the most absorbed sources (e.g. 3C 449, 3C 465; Capetti & Celotti 1999, Martel et al. 2000). In the most extreme cases (3C 270, 3C 296) the nuclear source is clearly visible in the optical, but it is not present in the UV. Such trend with orientation implies that the absorbing material cannot be distributed either as a spherical structure (all sources should be affected by absorption) nor as a thin disk where

the absorbing material is well confined. In the latter case, in fact, no trend with orientation should be seen: sources should be either absorbed or not absorbed without any intermediate case. However, the most striking difference between these structures and the classic AGN “tori” resides in the lower optical depth of the FR I absorbers, which allow us to observe the CCC even in the UV in all FR I, except for the most extreme cases of 3C 270 and 3C 296.

In light of these results, we can confirm the claim that FR I nuclei are generally unabsorbed. The moderate amount of absorption observed in these objects cannot be ascribed to the presence of a “classic” torus-like structure which is typical of other AGN, and might be instead accounted for either by extended (kpc-scale) dust lanes (e.g. in the case of 3C 29, in which the signature of a dust lane is clearly visible in the HST images, Sparks et al. 2000), or by the ( $\sim 100$  pc-scale) dusty disks. In the latter case, the absorbing column density must vary smoothly for different viewing angles.

As already noted above, one FR II (3C 388, which is classified as a LEG) lies in the region typical of FR I. This appears to confirm what has been already found in Paper II: 3C 388 belongs to a third class of FR II sources whose optical nuclei are indistinguishable from those of FR I (we have called such class “FR I-like”). The fact that this object is both on the radio-optical correlation and does not show any UV excess, typical of thermal disk emission, further constrains its origin as due to non-thermal synchrotron radiation, as it is for FR I nuclei. This also rules out the possibility that its CCC emission is produced by a compact scattering region, reflecting the presence of a hidden quasar in its nucleus, since quite flat values of  $\alpha_{o,UV}$  should be observed in that case. The synchrotron origin of its nuclear emission, together with the lack of strong emission lines in its spectrum, lead us to identify 3C 388 with a “parent source” for BL Lac objects, in agreement with the “dual population scheme” (Jackson & Wall 1999).

## 5.3. Variability

Spectral variability is a common characteristic of both synchrotron and disk-dominated sources. In particular, highly beamed non-thermal sources such as BL Lac objects show dramatic variations on all timescales (from minutes to years). Since

the relativistic beaming factor is expected to be significantly lower in radio galaxies, such behavior is expected to be present, although on longer timescales. Clearly, this might strongly affect the determination of the spectral slope. Therefore, it is important to use, where available, simultaneous observations.

Only three sources in our sample (3C 78, 3C 264, 3C 317) have simultaneous (within few hours) optical–UV data, while for 3C 274 the time lag between optical and UV observations is only  $\sim 6$  days. In addition to the FOC, 3C 317 has also been observed as part of the STIS UV SNAPSHOT program<sup>8</sup>. Interestingly, we have found that the flux of the CCC in the STIS observation is  $5.1 \times 10^{-17} \text{ erg cm}^{-2} \text{ s}^{-1} \text{ \AA}^{-1}$ , a factor of  $\sim 10$  brighter than in the FOC observation of 1994. Such high variability factor indeed strongly supports the non-thermal synchrotron scenario. Variability has been also detected in the optical band in 3C 274, although with much lower intensity (Tsvetanov et al. 1998).

The determination of the spectral slopes of objects for which no simultaneous data are available might be significantly affected by variability. However, we are confident that the general behavior of the CCC is correctly represented by our estimates. For the BLRG this is mainly supported by the fact that all of them show similar spectral indices. For the FR I, both their position in the plane of Fig. 4 and the close connection between steep  $\alpha_{o,UV}$  and the presence of obscuring structures are strong clues that obscuration and not variability is indeed the main physical reason for the observed steep slopes.

We conclude that the general behavior is well represented by the picture outlined above, although we cannot definitively rule out the possible presence of variability in individual sources.

## 6. Summary and conclusions

We have analyzed images of 28 nearby 3C radio galaxies for which both optical and UV HST images are available. We have found that all objects which show an UV CCC, also show it in the optical. Only two galaxies (of the FR I type)

which have a CCC do not have its UV counterpart. These missing nuclei seem to be associated with the presence of extended ( $\sim 100 \text{ pc}$ -scale) dusty disks which are seen almost edge-on in these galaxies, and might absorb the nuclear emission in the UV band. However, as the nuclei are clearly seen in the optical, the amount of absorption must be small, and not comparable to the much higher column densities characterizing absorbing “tori” in other classes of AGN. The high detection rate of unresolved nuclei in the UV among FR I sources further indicates that their nuclei are generally seen directly and absorbing tori are not a common characteristic among such low power radio galaxies.

Of the FR II, three are classified as broad-lined radio galaxies and show the brightest nuclei. The only non-broad lined FR II which shows a (fainter) CCC is 3C 388, which is classified as a LEG.

We have shown that by combining the UV data with the already available optical and radio information we can further investigate the origin of these nuclei. In a plane formed by the optical–UV spectral index versus the optical excess with respect to the radio core emission, CCC occupy different regions. This can be well explained if their position in such plane is strictly connected to the emission process. In particular, the bright nuclei of broad-lined FR II are explained with thermal emission from the accretion disk, while the other CCC (all FR I and one FR II, 3C 388) are compatible with being originated by synchrotron radiation from the jet. The strong variability found in the case of 3C 317 is a further clue of its synchrotron jet origin.

A major result of this work is that only a moderate amount of absorption, whose magnitude appears to be linked to the orientation of the source, is needed to account for the wide range of  $\alpha_{o,UV}$  spanned by FR I nuclei. Extinction can be higher than  $A_V \sim 1 - 2$  only in highly misoriented galaxies which clearly show extended dusty structures. This indeed constitutes the first direct evidence of nuclear absorption in FR I radio galaxies. Although supported by the presence of only one object, it appears that 3C 388 belongs to a class of FR II with FR I-like nuclei, in agreement with previous findings. In the framework of the unification models, these objects

<sup>8</sup>3C 317 was observed by STIS NUV-MAMA, with the F25SRF2 filter, on 1999 July 27.

might well represent the parent population of BL Lacs with an FR II radio morphology and power (Kollgaard et al. 1996; Cassaro et al. 1999).

FR II in which no nuclear source is seen are expected in the frame of the unification models, and we have found 11 FR II with no UV CCC which might be the obscured counterparts of BLRG. However, in order to firmly establish their role a detailed comparison of other properties of these sources (e.g. emission lines, X-ray spectra, extended power and morphology) with those of the unabsorbed FR II has to be carried out. If they indeed harbor an obscured quasar nucleus, these galaxies should also show strong IR nuclear components, as it has been found (at 10  $\mu$ m) for 3C 405 (Whysong & Antonucci 2001). Unfortunately, the incompleteness of the sample prevents us from drawing any conclusion on the geometry and covering factor of the obscuring material based on the relative number counts of obscured and unobscured objects.

These results provide further support for the idea that the nuclear structure of FR I is different from other AGN, in which signatures of the presence of nuclear optically thick dusty tori are often found. In these low power radio galaxies, the absorbing material cannot be distributed either as a spherical structure nor as a thin disk in which the absorbing material is well confined. The extended dusty disks often observed in such galaxies can well account for their observed properties. Having assessed the nature of the nuclear emission, the study of the possible connection between the extended dusty structures, the feeding mechanism of the central black hole and the nature of the accretion process in the different classes of radio galaxies is a promising future perspective for this work.

This work has been partially supported by the STScI (DDRF) grant D0001.82258. This research has made use of the NASA/IPAC Extragalactic Database (NED) which is operated by the Jet Propulsion Laboratory, California Institute of Technology, under contract with the National Aeronautics and Space Administration. The authors wish to thank the anonymous referee for useful comments and suggestions that improved the paper.

## REFERENCES

- Allen, M. G. A., Sparks, W. B., Koekemoer, A., Martel, A. R., O’Dea, C. P., Baum, S. A., Chiaberge, M., Macchetto, F. D., Miley, G. K., 2002, *ApJS*, in press
- Antonucci, R. R. J. & Ulvestad, J. S. 1985, *ApJ*, 294, 158
- Barthel, P. D. 1989, *ApJ*, 336, 606
- Capetti, A. & Celotti, A. 1999, *MNRAS*, 304, 434
- Cardelli, J. A., Clayton, G. C., & Mathis, J. S. 1988, *ApJ*, 329, L33
- Cassaro, P., Stanghellini, C., Bondi, M., Dallacasa, D., della Ceca, R., & Zappalà, R. A. 1999, *A&AS*, 139, 601
- Chiaberge, M., Capetti, A., & Celotti, A. 2002, *A&A*, submitted
- Chiaberge, M., Capetti, A., & Celotti, A. 2000, *A&A*, 355, 873, (Paper II)
- Chiaberge, M., Celotti, A., Capetti, A., & Ghisellini, G. 2000b, *A&A*, 358, 104
- Chiaberge M., Capetti A., Celotti A. 1999, *A&A*, 349, 77, (Paper I)
- Elvis, M. et al. 1994, *ApJS*, 95, 1
- Fossati, G., Maraschi, L., Celotti, A., Comastri, A., & Ghisellini, G. 1998, *MNRAS*, 299, 433
- Ghisellini, G., Celotti, A., Fossati, G., Maraschi, L., & Comastri, A. 1998, *MNRAS*, 301, 451
- Giovannini, G., Feretti, L., Gregorini, L., & Parma, P. 1988, *A&A*, 199, 73
- Hine, R. G. & Longair, M. S. 1979, *MNRAS*, 188, 111
- Jackson, N. & Rawlings, S. 1997, *MNRAS*, 286, 241
- Jackson, C. A. & Wall, J. V. 1999, *MNRAS*, 304, 160
- Kollgaard, R. I., Palma, C., Laurent-Muehleisen, S. A., & Feigelson, E. D. 1996, *ApJ*, 465, 115
- Martel, A. ;., Turner, N. J., Sparks, W. B., & Baum, S. A. 2000, *ApJS*, 130, 267

- Marconi, A., Schreier, E. J., Koekemoer, A.,  
Capetti, A., Axon, D., Macchetto, D., & Caon,  
N. 2000, *ApJ*, 528, 276
- Narayan, R. & Yi, I. 1995, *ApJ*, 444, 231
- Perlman, E. S., Sparks, W. B., Radomski, J.,  
Packham, C., Fisher, R. S., Piña, R., & Biretta,  
J. A. 2001, *ApJ*, 561, L51
- Rees, M. J., Phinney, E. S., Begelman, M. C., &  
Blandford, R. D. 1982, *Nature*, 295, 17
- Sparks, W. B., Baum, S. A., Biretta, J., Mac-  
chetto, F. D., & Martel, A. ;. 2000, *ApJ*, 542,  
667
- Tsvetanov, Z. I., Hartig, G. F., Ford, H. C., et al.  
1998, *ApJ*, 493, L83
- Urry, C. M., Padovani, P. 1995, *PASP*107, 803
- Whysong, D., Antonucci, R. R. J., *astro-*  
*ph/0106381*
- Zirbel, E. L. & Baum, S. A. 1995, *ApJ*, 448, 521